Band-selective gap opening by a C_4-symmetric order in a proximity-coupled heterostructure Sr_2VO_3FeAs

Sunghun Kim[a,1], Jong Mok Ok[b,c,1], Hanbit Oh[a], Chang Il Kwon[b,c], Yi Zhang[d,e], Jonathan D. Denlinger[e], Sung-Kwan Mo[e], Frederik Wolff-Fabris[f], Erik Kampert[f], Eun-Gook Moon[a,2], Changyoung Kim[g,h,2], Jun Sung Kim[b,c,2], and Yeongkwan Kim[a,2]

[a]Department of Physics, Korea Advanced Institute of Science and Technology, Daejeon 34141, Republic of Korea; [b]Center for Artificial Low Dimensional Electronic Systems, Institute for Basic Science, Pohang 37673, Republic of Korea; [c]Department of Physics, Pohang University of Science and Technology, Pohang 37673, Republic of Korea; [d]National Laboratory of Solid State Microstructures, School of Physics, Collaborative Innovation Center of Advanced Microstructures, Nanjing University, Nanjing 210093, China; [e]Advanced Light Source, Lawrence Berkeley National Laboratory, Berkeley, CA 94720; [f]Dresden High Magnetic Field Laboratory, Helmholtz-Zentrum Dresden-Rossendorf, Dresden D-01314, Germany; [g]Center for Correlated Electron Systems, Institute for Basic Science, Seoul 08826, Republic of Korea; and [h]Department of Physics and Astronomy, Seoul National University, Seoul 08826, Republic of Korea

Edited by Zachary Fisk, University of California, Irvine, CA, and approved October 19, 2021 (received for review March 17, 2021)

Complex electronic phases in strongly correlated electron systems are manifested by broken symmetries in the low-energy electronic states. Some mysterious phases, however, exhibit intriguing energy gap opening without an apparent signature of symmetry breaking (e.g., high-T_C cuprates and heavy fermion superconductors). Here, we report an unconventional gap opening in a heterostructured, iron-based superconductor Sr_2VO_3FeAs across a phase transition at T_0 ∼150 K. Using angle-resolved photoemission spectroscopy, we identify that a fully isotropic gap opens selectively on one of the Fermi surfaces with finite warping along the interlayer direction. This band selectivity is incompatible with conventional gap opening mechanisms associated with symmetry breaking. These findings, together with the unusual field-dependent magnetoresistance, suggest that the Kondo-type proximity coupling of itinerant Fe electrons to localized V spin plays a role in stabilizing the exotic phase, which may serve as a distinct precursor state for unconventional superconductivity.

strong electron correlation | heterostructure | proximity coupling | iron-based superconductors

Strongly correlated electron systems often exhibit a variety of self-organized forms with broken symmetry. Particularly, in correlated itinerant electron systems, exemplified by doped copper- and iron-based superconductors (FeSCs) (1, 2), multiple many-body instabilities promote rich and complex landscape of electronic orders, including different types of spin, charge, or orbital orders. The resulting broken symmetry renders the footprint in the electronic structure such as band folding, band splitting, and the gap opening. Investigating those footprints thus in turn provides characteristics of phase—what type of phase transition occurs, what kind of interaction is involved, and how the system lowers the energy across the phase transition. For instance, an anisotropic gap opening only at a segment of the Fermi surface (FS) indicates the breaking of translational symmetry and thus suggests a density wave and spin ordering as the corresponding phase (3–5). An isotropic gap opening, on the other hand, can be attributed to a phase without translational symmetry breaking, such as Mott phase. In addition, the loss of coherent spectral weight near the Fermi level could allow us to determine the underlying interaction, such as strong electron correlation (6–9) and coupling with local magnetic moment (10, 11).

Recently, in a correlated heterostructure system Sr_2VO_3FeAs, a mysterious phase transition is found to occur at T_0 ∼150 K. The order parameter and thus symmetry of the phase are still elusive, despite the clear thermodynamic evidences for its existence. The system is composed of iron arsenide (SrFeAs) and Mott-insulating transition metal oxide ($SrVO_3$) layers (Fig. 1 *A* and *B*) (12–14). The two constituent layers are known to favor distinct C_2 and C_4 symmetric magnetic phases, respectively. Through a proximity coupling, however, localized spins in the $SrVO_3$ layers are expected to couple with Fe 3*d* electrons in the FeAs layers and obtain strong magnetic frustration, which may lead to a transition to a distinct phase. Indeed, recent experimental investigations revealed that the known magnetic phases such as collinear antiferromagnetic (AF) or nematic order of SrFeAs layer and Néel-type AF order in $SrVO_3$ layer are not stabilized in this system (15). Furthermore, no evidence of time-reversal or lattice symmetry breaking has been observed across this mysterious phase transition (15–17), suggesting an intriguing intraunit cell order with C_4 symmetry.

To understand this mysterious phase transition, it is desired to investigate the electronic structure evolution across the transition. Here, via systematic temperature-dependent angle-resolved photoemission spectroscopy (ARPES) studies, we show that the transition accompanies an isotropic gap opening on only one of the FSs with strong interlayer hopping. Our measurements reveal that the lattice C_4 and time-reversal symmetries are retained across the phase transition, which is incompatible with known gap opening mechanisms such as band-selective Mott (6–9) or spin/charge density-wave transitions (3–5). The band selectiveness, which should be from the

Significance

Heterostructures of correlated electronic systems offer versatile platforms for various types of quantum phases and their transitions. A common wisdom states that the proximity coupling between constituent layers plays a secondary role, because it is much weaker than the intralayer interactions. In this work, we present a counterexample of the belief. Namely, the proximity coupling between localized spins and itinerant electrons stabilizes an exotic electronic state with band-selective gap opening whose observation is done in a correlated heterostructure Sr_2VO_3FeAs. Our finding highlights that the proximity coupling can be an effective knob for exotic phases in correlated heterostructures.

Author contributions: E.-G.M., C.K., J.S.K., and Y.K. designed research; S.K., J.M.O., H.O., C.I.K., Y.Z., J.D.D., S.-K.M., F.W.-F., E.K., E.-G.M., J.S.K., and Y.K. performed research; S.K., J.M.O., H.O., E.-G.M., J.S.K., and Y.K. analyzed data; and S.K., E.-G.M., C.K., J.S.K., and Y.K. wrote the paper.

The authors declare no competing interest.

This article is a PNAS Direct Submission.

[1]S.K. and J.M.O. contributed equally to this work.

[2]To whom correspondence may be addressed. Email: egmoon@kaist.ac.kr, changyoung@snu.ac.kr, js.kim@postech.ac.kr, or yeongkwan@kaist.ac.kr.

This article contains supporting information online at http://www.pnas.org/lookup/suppl/doi:10.1073/pnas.2105190118/-/DCSupplemental.

Published November 17, 2021.

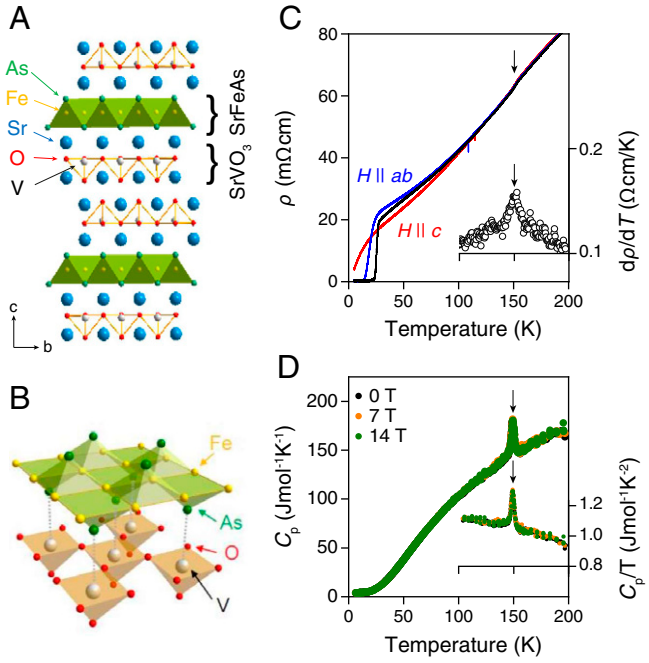

Fig. 1. Crystal structure of Sr_2VO_3FeAs and the anomalous phase transition. (*A* and *B*) The crystal structure of Sr_2VO_3FeAs, a natural heterostructure with $[SrFeAs]^{+1}$ and $[SrVO3]^{-1}$ layers. In the $[SrVO3]^{-1}$ layers, V ions form a network of corner-sharing tetrahedrons, while the FeAs layers consist of edge-sharing $FeAs_4$ tetrahedrons. The As atoms below the center of the Fe_4 units of the FeAs layer are placed on top of the V atoms in the neighboring $SrVO_3$ layers, thus bridging the Fe and the V planes as indicated by the dashed lines in *B*. For clarity, the Sr atoms between these layers are removed in *B*. (*C*) The resistivity in the *ab* plane (ρ_{ab}) shows a clear anomaly at T_0 ~150 K, which becomes more clear in its temperature derivative $d\rho_{ab}(T)/dT$ shown in the *Inset*. With a magnetic field along $H \parallel ab$ or $H \parallel c$, no shift or broadening is observed in either $\rho_{ab}(T)$ or $d\rho_{ab}(T)/dT$ curve. The drop in resistivity below 30 K represents the superconducting transition. (*D*) The specific heat C_p of Sr_2VO_3FeAs as a function of temperature at $H = 0$, 7, and 14 T. A sharp peak without magnetic field dependence is observed at T_0. The *Inset* shows $C_p(T)/T$ near the phase transition at T_0.

interlayer hopping strength, together with an unusual magnetoresistance (MR) below T_0 emphasizes the importance of proximity coupling with localized V spins to induce the exotic C_4 symmetric ordered phase. This phase may serve as a distinct parent state for superconductivity in Sr_2VO_3FeAs, in which the usual pairing channel is suppressed by the gap opening.

Results

An intriguing phase transition at T_0 ~150 K is clearly indicated by the temperature-dependent resistivity $\rho(T)$ (Fig. 1*C*) and specific heat $C_P(T)$ (Fig. 1*D*) of our single crystalline samples. Neither thermal hysteresis nor magnetic field dependence in T_0 is observed in $\rho(T)$ up to 14 T, whereas significant MR develops below T_0 as we discuss below. The anomaly in $C_P(T)$ is sharper than expected in the mean-field behavior of the conventional second order transition, indicating the weakly first-order character. As compared to typical phase transitions found in FeSCs, the observed specific-heat anomaly is sharper than at the nematic transition but smoother than at the magnetic transition in other FeSCs (18, 19), showing significant coupling with lattice degree of freedom (20). In Sr_2VO_3FeAs, a sudden drop of the *c*-axis lattice parameter at T_0 indicates a sizable coupling of the *c*-axis lattice contraction to the phase transition (15). No evidence for broken tetragonal C_4 or time-reversal symmetry across T_0 was found in a recent nuclear magnetic resonance (NMR) study using both As and V nuclei (15). Also, no additional Bragg peak observed in X-ray and neutron diffraction patterns indicates intact translational symmetry across T_0 (15–17). Therefore, despite the clear thermodynamic signature of the phase transition as shown in Fig. 1, the phase transition cannot be described by the conventional magnetic, nematic, or density-wave ordering reported in other FeSCs (21, 22).

To understand the electronic response across the intriguing transition, we study the low-energy electronic structure using ARPES. Since the Mott-insulating $SrVO_3$ layers do not contribute to low-energy states near the Fermi energy (E_F) (23, 24), the overall electronic structure of Sr_2VO_3FeAs shown in Fig. 2 *A* and *B* follows the general band topology of other FeSCs (21, 22, 25). There are three bands centered at the Γ point, one electron band (α) and two hole bands (β and γ), while two electron bands (δ and ε) are located at the *M* point of the Brillouin zone (BZ). For each band, the contributions from Fe orbitals (mostly d_{xz}, d_{yz}, and d_{xy}) differ, as summarized by the color-coded lines in Fig. 2*C*, which is determined by the systematic, polarization-dependent ARPES study (24). The orbital characters of these bands are similar to those of other FeSCs except for the γ hole band. For other FeSCs, the γ hole band near E_F is derived almost entirely from the in-plane d_{xy} orbital and shows a strong two-dimensional character. However, the γ hole band of Sr_2VO_3FeAs was found to be comprised of all three t_{2g} orbitals, which leads to the finite k_z dispersion. In terms of energy, the band disperses within the relatively small range of about 10 meV, as illustrated in Fig. 2*C* with thickness. Since the γ hole band top is located close to E_F, it can provoke the rather significant k_z warping of the γ hole pocket (i.e., even stronger than that of δ and ε electron pockets) (*SI Appendix*, Fig. S1). This unusual orbital mixing and the resulting k_z dispersion of the γ hole band are critical to its response across T_0. Such behavior is distinct from that of other FSs, as discussed below.

As well as identify the overall band structure of Sr_2VO_3FeAs, we also investigate the detailed low-energy electronic structure near the E_F. We first compare gap opening in the electron (δ and ε) and hole (γ) bands (Fig. 2 *D* and *E*). The symmetrized energy distribution curves (EDCs) taken at T ~14 K (i.e., well below the T_C of ~30 K) exhibit a clear gap for both the δ electron and γ hole bands. The gap sizes for the δ and γ bands, estimated with the Dynes formula, differ significantly from each other, as shown in Fig. 2*F* (Δ_δ ~10 meV and Δ_γ ~35 meV for electron and hole bands, respectively). A gap is also observed for the small α electron band, and its size follows the superconducting gap function $\Delta = \Delta_0|\cos k_x \cos k_y|$, together with that of the δ band (*SI Appendix*, Fig. S3). The gap in the δ electron band obtained from the temperature-dependent spectra (Fig. 2*D*) follows the Bardeen-Cooper-Schrieffer (BCS)-like temperature evolution and closes at T_C (Fig. 2*F*). $2\Delta/k_BT_C$ is found to be ~8, which is a typical value for strongly coupled superconductors.

In contrast to the gap behavior of electron bands, surprisingly, the size of the larger gap in the γ hole band remains similar across T_C (Fig. 2 *E* and *F*). To investigate the behavior of the anomalous gap in the γ hole band, we obtained data at higher temperatures, in the range between 70 and 170 K, as shown in Fig. 2*G*. We take the polynomial fit of the spectrum at 170 K as the normal-state spectrum and overlay them as dashed lines in Fig. 2*G*. First, compared to the normal-state spectrum, it should be noted from the 70 K data are that the spectral weight is transferred within the narrow energy range from E_F to a peak at a higher binding energy of ~40 meV, forming a gap with a full suppression of spectral weight at E_F (*SI Appendix*, Fig. S4). The overlaid spectra in Fig. 2*H* clearly show that the gap is gradually filled, and the peak is suppressed as the temperature increases past T_C. Both the gap and peak finally disappear near T_0 ~150 K (Fig. 2*I* and *SI Appendix*, Fig. S5). A clear "peak-and-gap" line shape is the key feature distinct from the

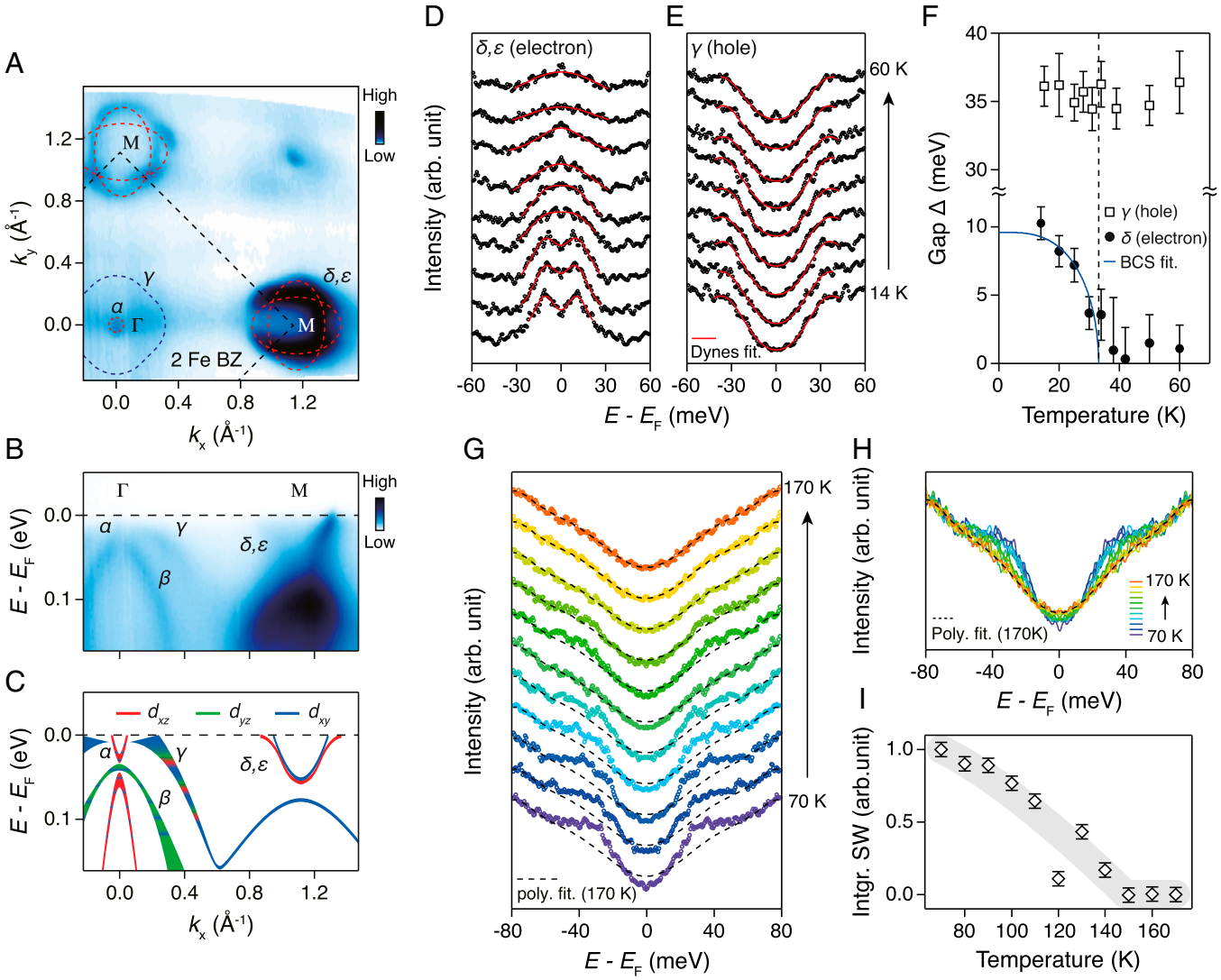

Fig. 2. Electronic structure of Sr_2VO_3FeAs and anomalous temperature-dependent gap. (*A*) FS map of Sr_2VO_3FeAs observed by ARPES. Red and blue dashed lines overlaid on the figure represent electron (α, δ, and ε) and hole (γ) FSs, respectively. The black dashed line represents BZ in the two-Fe unit cell. (*B*) Band structure along the (0,0)-(π,0) direction. (*C*) Schematic of the band structure with color-coded lines corresponding to orbital contributions (d_{xz}, d_{yz}, and d_{xy}). (*D* and *E*) Symmetrized EDCs from Fermi momenta (k_F) of electron (δ and ε) and hole (γ) bands, respectively, for different temperatures. The overlaid red curves are the results of the Dynes formula fits. (*F*) Gap sizes obtained by applying the Dynes formula fit to the data in *D* and *E* as a function of temperature. The error bars include the uncertainty in the position of the E_F. (*G*) Symmetrized EDCs of the γ hole band for temperatures between 70 and 170 K. Overlaid, black dashed lines are the polynomial fit of the 170 K spectrum. (*H*) The spectra in *G* are overlaid on top of each other to show the temperature evolution more clearly. (*I*) Integrated spectral weight of the difference between the data and polynomial fit of the 170 K spectrum as a function of the temperature. The integrated spectral weight of 70 K is normalized to 1.

so-called pseudogap behavior of other FeSCs (26, 27) and high-T_C cuprates (28, 29)—a partial gap feature only due to spectral weight transfer to a much-wider energy window. We can see that the gap size has little temperature dependence, which is in contrast to the gap evolution expected in the mean-field theory but is consistent with the sharp anomaly in the specific-heat data (Fig. 1*D*). These observations unambiguously reveal that across T_0, unusual electronic gap opening occurs in the hole Fermi pocket with a gap ratio $2\Delta/k_BT_0 \sim 6$, while the electron pockets remain gapless above T_C.

Having established that the unusual band-selective gap opening occurs only in the hole pocket below T_0, we now examine the in-plane momentum dependence of the gap to determine whether there is any signature of C_4 symmetry breaking in the gap structure related to the phase transition. Fig. 3*A* depicts symmetrized EDCs taken along the hole FS (Fig. 3*C*) at $T = 60$ K ($T_C < T < T_0$) for $k_z = 0$. Note that the peak-and-gap feature is present in all of the spectra, that is, in all directions. The gap sizes of the spectra are again estimated with the Dynes fit, as indicated by the overlaid curves in Fig. 3*A*, and the results are plotted in Fig. 3*C*. The anomalous gap at $T_C < T < T_0$ is almost independent of the in-plane momentum. Assuming a possible azimuthal angle (ϕ) dependence in the k_x-k_y plane, expressed by $\Delta(\phi) = \Delta_0 + \Delta_n \cos n\phi$, the n-fold gap anisotropy Δ_n should be less than ~5% of isotropic gap Δ_0.

It is still conceivable that the gap may not be isotropic at other k_z values, as there is fairly large k_z dispersion for the γ hole pocket (24); the ARPES intensity map at the binding energy of 10 meV in the k_z-$k_{||}$ plane near the BZ center in Fig. 3*D* indeed clearly shows that the γ hole pocket has k_z dispersion (*SI Appendix*, Fig. S1). We therefore took the same set of γ hole band gap data for $k_z = \pi$ and plotted these in Fig. 3*B*. The

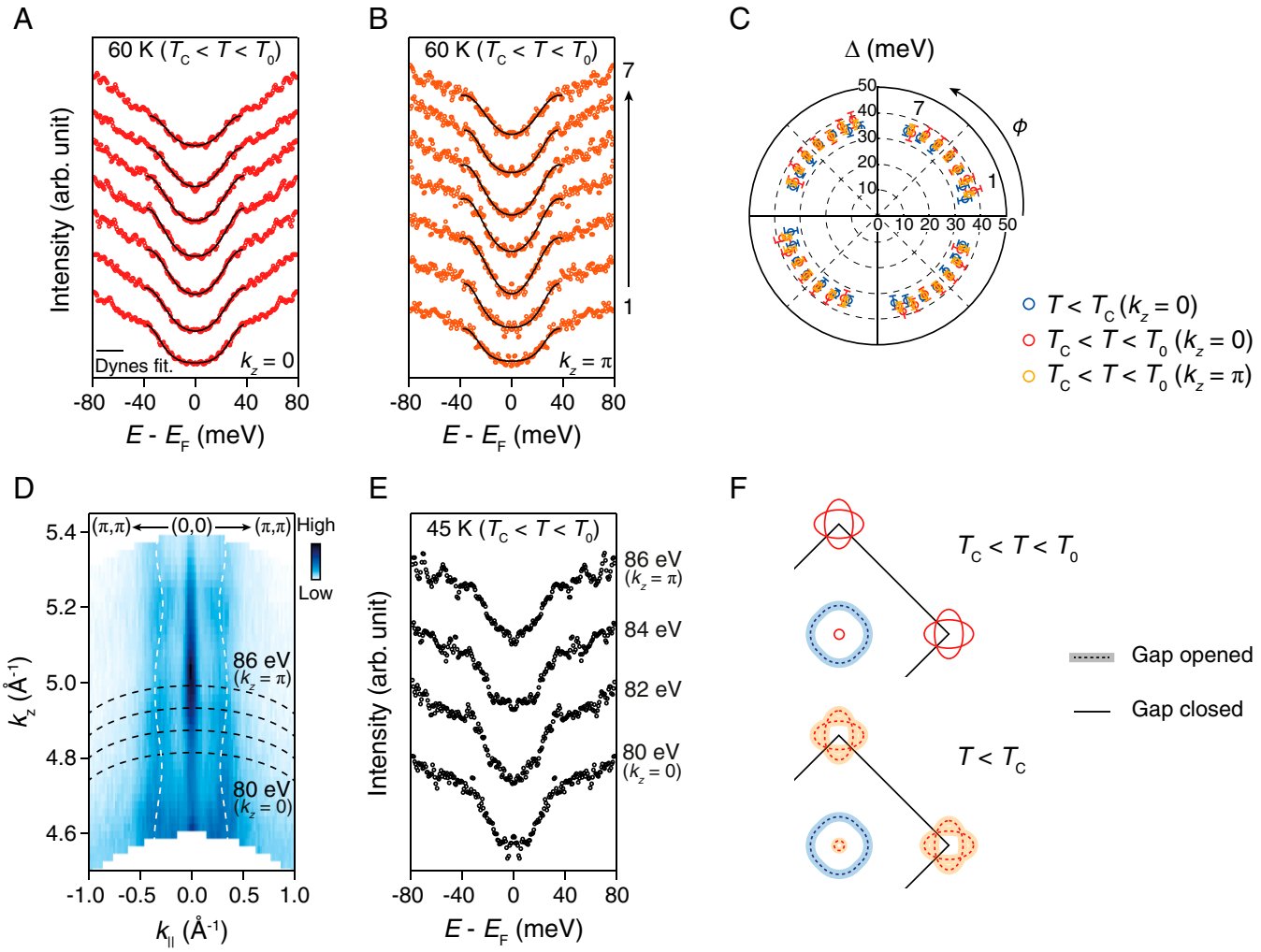

Fig. 3. Isotropic and k_z-independent gap in the hole band. (*A* and *B*) Symmetrized EDCs from different momenta on the hole FS for the $k_z = 0$ (*A*) and $k_z = \pi$ (*B*) planes at $T = 60$ K ($T_C < T < T_0$). Overlaid, black solid curves are the results of the Dynes formula fit. (*C*) The gap size for different k_z and temperatures as a function of azimuthal angle (ϕ) with respect to the k_x axis. Only the data points in the first quadrant are actual data points; those in the other quadrants are derived from symmetrization. (*D*) k_z dispersion along the (0,0)-(π,π) direction near the BZ center. White dashed lines are drawn as a guide for the eye for γ hole band dispersion. (*E*) Symmetrized EDCs from the hole band at different photon energies (80, 82, 84, and 86 eV). The corresponding k_z positions are denoted by black dashed lines in *D*. All spectra are taken at 45 K between T_C and T_0. (*F*) Schematic illustration of the gap behavior for hole and electron FSs at two different temperatures, $T_C < T < T_0$ (*Upper*) and $T < T_C$ (*Lower*).

peak-and-gap feature is developed below T_0 (*SI Appendix*, Fig. S6), as is the case for the symmetrized EDCs taken at $k_z = 0$ (Fig. 3*A*). The procedure used to extract the gap from the $k_z = 0$ data yields an isotropic gap for $k_z = \pi$, as plotted in Fig. 3*C*. It should be noted that the gap sizes for $k_z = 0$ and π are almost the same, as shown in Fig. 3*C*. The EDCs taken with various photon energies between $h\nu = 80$ and 86 eV (corresponding k_z values are indicated by the black dashed lines in Fig. 3*D*) are also found to have essentially the same gap size (Fig. 3*E*). The observed anomalous gap above T_C is therefore independent of both the in-plane and out-of-plane momentum, indicating a fully isotropic gap in the γ pocket. The fully isotropic gap confirms that the rotational and translational symmetries of the underlying crystal lattice are retained across T_0, consistent with the results of previous studies (15).

The observed, anomalous, full gap opening cannot easily be explained by conventional mechanisms of gap opening. In particular, the band-selective and fully isotropic gap opening set strong constraints on its origin. The isotropic gap in the γ pocket, centered at the Γ point, together with the lack of splitting of degenerate d_{xz} and d_{yz} states of δ and ε bands (Fig. 2*B* and *SI Appendix*, Fig. S7), reflects the C_4 symmetry of the tetragonal lattice maintained in the FeAs layers across T_0. This is consistent with the nearly isotropic Knight shift at T_0 seen in the recent NMR study (15) and thus clearly rules out the C_2 nematic order, which is one of the most common orders in FeSCs (21, 22). A band-selective Mott transition, which is often found in FeSCs (6–9), is also unlikely. In a band-selective Mott transition, a particular heavy band loses its coherent spectral weight and becomes localized due to the strong electron correlation effect, while the other bands remain itinerant. In this case, as found for the d_{xy} bands in $K_xFe_{2-y}Se_2$ (6–8), the spectral weight is completely suppressed for the entire band in the whole BZ and is transferred to the Hubbard state located far away from E_F by $\sim U$, which is much larger than the bandwidth. In Sr_2VO_3FeAs, however, spectral weight transfer occurs only near E_F, within an energy window much smaller than the bandwidth; the rest of γ band remains almost intact.

Furthermore, the almost isotropic gap over the whole γ FS (Fig. 3*C*) is also inconsistent with the conventional density-wave

transitions. In density wave–type transitions with a nonzero $\boldsymbol{Q}$ modulation, for example, strong gap opening occurs at sections of FS that are connected with the modulation vector $\boldsymbol{Q}$, leading to significant gap anisotropy in momentum space (3–5). As shown in our simulations based on mean-field theory for a density-wave order with $\boldsymbol{Q}$ = (π,0) or (0,π), the relative gap anisotropy with respect to the isotropic gap Δ_n/Δ_0 is larger than ∼1 (*SI Appendix*, Fig. S13), clearly distinct from our experimental results. The remaining candidates are associated with an intraunit cell order with a zero $\boldsymbol{Q}$, which are often called vestigial phases of a C_4 symmetric double-$\boldsymbol{Q}$ spin order (30, 31). These phases are described by composite spin-orbital order patterns, retaining the C_4 symmetry. However, even in these phases, characteristic band shift or splitting rather than gap opening is expected to occur, in stark contrast to experimental results as summarized in Fig. 3*F*. Thus, the selective gap opening only at the γ hole pocket is highly nontrivial and inconsistent with theoretical models describing the various phases due to the broken symmetry known or proposed in FeSCs so far.

While the relevant symmetry breaking of the gap opening is unclear, its band selectiveness may further provide a clue regarding the nature of the C_4 symmetric order. In other FeSCs, the γ hole pocket mainly arises from the d_{xy} orbital, which is believed to have a stronger correlation effect than $d_{xz,yz}$-related bands (22, 32). In Sr_2VO_3FeAs, however, there are significant contributions from $d_{xz,yz}$ orbitals to the γ hole pocket, which thus shows finite dispersion along the k_z direction. This contrasts with the δ and ε electron pockets at the M point, which have negligible k_z warping with strong two-dimensionality. The α electron pocket at the Γ point appears to have a weak k_z dispersion compared to the γ hole pocket. These two-dimensional FSs—α, δ, and ε pockets—remain gapless below T_0 until superconductivity develops below T_C; that is, the full gap below T_0 selectively develops at the γ hole pocket that has a distinctive k_z dispersion and thus strong interlayer hopping. This suggests that proximity coupling to the neighboring Mott-insulating layers plays an important role in triggering the C_4 symmetric state.

The importance of the proximity coupling is also reflected in the unusual transport properties seen under magnetic fields. Fig. 4 shows the in-plane MR, $\rho_{ab}(H)$, under magnetic fields of up to 60 T for $H \parallel ab$ and $H \parallel c$ in the transverse configuration. At high temperatures above T_0, positive MR is seen for both $H \parallel c$ and $H \parallel ab$, with that for $H \parallel c$ being slightly larger. This can be understood in terms of the conventional orbital effect typically found in quasi–two-dimensional systems (*SI Appendix*, Fig. S8). However, an additional contribution of the negative MR starts to emerge for $H \parallel c$ below T_0, and dominates the field dependence until it is saturated at higher magnetic fields. Taking the MR for $H \parallel ab$ as the reference, we estimate the negative contribution of the MR for $H \parallel c$ by $\Delta\rho_{ab} = \rho_{ab}(H \parallel c) - \rho_{ab}(H \parallel ab)$ at H = 60 T, which shows a clear onset at T_0 (Fig. 4*H*). The similar behavior is also observed in the longitudinal MR along the c-axis, as shown in $\Delta\rho_c(H) = (\rho_c(H) - \rho_c(0))/\rho_c(0)$ for $H \parallel c$ (*SI Appendix*, Fig. S9). The negative contribution in MR is clearly developed below T_0, further confirming that observed unusual MR is not due to the orbital effect. Such negative MR has not been observed in any FeSCs, except $EuFe_2As_2$ (33), in which the spin scattering due to localized Eu spins above T_N is important. The observed complex, field-dependent MR in Sr_2VO_3FeAs below T_0 can only be understood by taking into account the significant scattering of itinerant electrons with fluctuating localized spins, which is suppressed under high magnetic fields. This shows that the phase transition across T_0 in Sr_2VO_3FeAs is intimately tied to the hybridization between the itinerant Fe electron fluid and localized V spins caused by proximity coupling.

In Sr_2VO_3FeAs, the localized V spins are known to remain fluctuating at least down to 5 K, even with a large Curie–Weiss temperature (Θ ∼100 K) (15, 16, 34). The absence of magnetic order for V spins in the square lattice by itself evidences additional Kondo-like coupling J_K with Fe electrons across the interface, which is frustrated with the intralayer superexchange interaction J_{ex} of localized V spins (15). This is consistent with the enhancement of the interlayer J_K interaction across T_0 observed in the MR behavior as shown in Fig. 4. A significant spin interaction between the SrFeAs and the $SrVO_3$ layers is also captured in recent measurements of the spin relaxation time, which showed a spin-gap–like behavior with unusual suppression of the stripe-type AF fluctuation (15). Furthermore, we found that T_0 systematically increases with external pressure (Fig. 4*I* and *SI Appendix*, Fig. S10). External pressure mostly reduces the interlayer distance and thus enhances proximity coupling in layered compounds like Sr_2VO_3FeAs. This pressure dependence is consistent with the notion that the hybridization between itinerant electron in the FeAs layers and the localized spin in the $SrVO_3$ layers is responsible for stabilizing the C_4 symmetric state.

Discussion

Based on these results, we show that the observed band-selective gap opening is independent of symmetry breaking. Employing the highest two-dimensional group on a square lattice, we consider all possible subgroups and investigate the effect of their breaking on band structures (*SI Appendix*, Table S3). The resulting energy gap opening either occurs in both electron and hole bands or becomes highly anisotropic in the momentum space, which is in sharp contrast to our experimental observations. Thus, we conclude that any symmetry-breaking channels cannot explain the band-selective, fully isotropic gap opening in Sr_2VO_3FeAs.

Although the precise mechanism of the observed exotic gap opening that preserves the symmetry of normal phase is yet to be identified, we stress that the very existence of the exotic gap opening indicates importance of the Kondo-like proximity coupling between itinerant Fe 3*d* electron and localized V spins. Since itinerant electrons in SrFeAs layer are spatially separated from the localized spins in $SrVO_3$ layer and coupled through As orbitals (Fig. 1*B*), the coupling J_K is essentially nonlocal. It can thus introduce strong momentum-space anisotropy in hybridization (35, 36). In addition, itinerant Fe electrons have an internal orbital degree of freedom, particularly in the γ hole band with highly mixed $3d_{xz,yz}$ and $3d_{xy}$ orbitals. These nonlocal and multiorbital features may play a role in the abrupt change in J_K across T_0, which could lead to the band-selective gap opening (Fig. 2), the onset of negative MR (Fig. 4), and a reduction in the c-axis lattice parameter (15).

Our results suggest the important role of the magnetic proximity coupling, while it leaves several interesting open questions. Recently, the Jacarrino–Peter effect has been observed in the upper critical fields of Sr_2VO_3FeAs, revealing that the interlayer coupling J_K ∼2 meV is AF (37). The relatively small J_K, as compared to the observed gap energy scale Δ ∼30 meV, implies that interactions with larger energy scales are involved in the phase transition. Magnetic exchange interactions in the FeAs and VO_3 layers are generally expected to be ∼50 meV (38) and ∼10 meV (39, 40), respectively. The energy scale of orbital ordering in FeSCs is ∼50 meV (41), while that in RVO_3 (R = rare earth ion or Y) is in the range of 50 to 100 meV (40). We stress that the symmetry broken phases associated with those larger energy scales are not stabilized in the present heterostructure, which could lead to a nonlinear dependence of the gap on J_K as found in correlated systems such as quantum criticality (42, 43) and Kondo effect (44).

PHYSICS

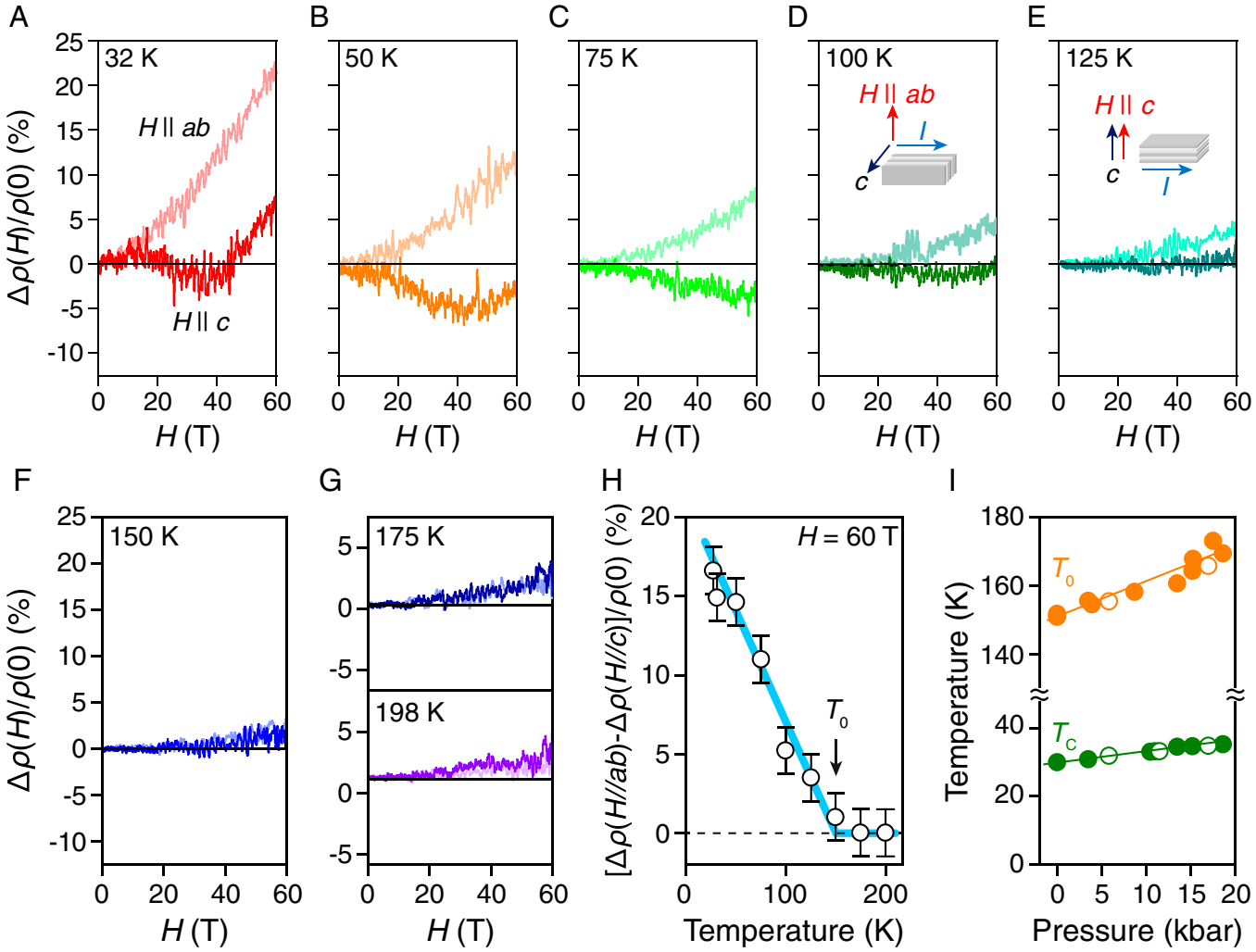

Fig. 4. Negative MR and pressure tuning. (*A–G*) Magnetic field–dependent MR $\Delta\rho(H)/\rho(0)$ of Sr_2VO_3FeAs up to 60 T at various temperatures for $H \parallel ab$ and $H \parallel c$. The *Inset* shows a schematic of current and field orientation with respect to the *c*-axis. The negative MR for $H \parallel c$, which developed below T_0, is distinct from the strong positive MR for $H \parallel ab$. (*H*) The anisotropy of the MR, given by the difference between $\Delta\rho(H \parallel ab)$ and $\Delta\rho(H \parallel c)$, normalized by $\rho(0)$ as a function of temperature. The onset of anisotropic MR well matches T_0. (*I*) Pressure dependence of T_0 and T_C.

Furthermore, the band-selective gap opening is expected to affect the superconducting properties in the FeAs layers significantly. Below T_0, the γ hole FS disappears, and the typical superconducting pairing channel connecting the γ hole and the δ and ε electron FSs is suppressed. This can invoke other pairing interactions [e.g., with the incipient β hole bands (45, 46) or via other C_4 symmetric AF fluctuations (30)]. The possibility of more exotic scenarios associated with deconfined phases, such as fractionalized Fermi liquids and orthogonal metals (47–50) for the mysterious order and the coexistence of a superconducting order, remains to be explored. Our findings regarding the C_4 symmetric order of Sr_2VO_3FeAs highlight that interfacing 3*d* transition pnictides and oxides could host diverse exotic phases with entangled spin, orbital, and charge degrees of freedom in tunable manner through proximity coupling.

Materials and Methods

Single Crystal Growth. Sr_2VO_3FeAs single crystals were grown using self-flux techniques as follows. The mixture of SrO, VO_3, Fe, SrAs, and FeAs powders with a stoichiometry of Sr_2VO_3FeAs:FeAs = 1:2 was pressed into a pellet and sealed in an evacuated quartz tube under Ar atmosphere. The sample were heated to 1,180 °C, held at this temperature for 80 h, cooled slowly first to 950 °C at a rate of 2 °C/h, and then furnace-cooled. The plate-shaped single crystals were mechanically extracted from the flux. High crystallinity and stoichiometry are confirmed by the X-ray diffraction and energy-dispersive spectroscopy. The typical size of the single crystals is $200 \times 200 \times 10\ \mu m^3$.

Transport Properties and Specific Heat. Magnetotransport properties were measured using conventional four-probe configuration on a single crystal in a 14-T Physical Property Measurement System (Quantum Design), a 33-T Bitter magnet at the National High Magnetic Field Laboratory, Tallahassee, and a 60-T pulse magnet at Dresden High Magnetic Field Laboratory, Dresden. Specific-heat measurements were done on several pieces of Sr_2VO_3FeAs single crystals (~1 mg) using the relaxation method in a 14-T Physical Property Measurement System (Quantum Design).

ARPES. ARPES measurements were performed at beam lines 10.0.1 and 4.0.3 of the Advanced Light Source, Lawrence Berkeley National Laboratory. Samples were cleaved at 10 K in an ultra-high vacuum better than 3×10^{-11} Torr. Spectra were acquired with Scienta R4000 analyzer at beam line 10.0.1 and Scienta R8000 analyzer at beam line 4.0.3. Several photon energies, particularly between 40 and 70 eV at beam line 10.0.1 and between 68 and 100 eV at beamline 4.0.3, were used for the ARPES measurements including photon energy dependence. The overall energy resolution was 18 meV or better.

Data Availability. All study data are included in the article and/or *SI Appendix*.

ACKNOWLEDGMENTS. We thank I. Mazin, S.-H. Baek, H. W. Yeom, and Y. Bang for fruitful discussion. The work at Korea Advanced Institute of Science and Technology was supported by the National Research Foundation of

Korea (NRF) with Grant Nos. 2015M3D1A1070672, 2020K1A3A7A09080366, 2020R1A4A2002828, 2021R1A2C1013119, 2019R1A6A1A10073887, 2019M3E4A1080411, 2020R1A4A3079707, and 2021R1A2C4001847. The work at Pohang University of Science and Technology (POSTECH) was supported by the Institute for Basic Science (IBS) through the Center for Artificial Low Dimensional Electronic System (No. IBS-R014-D1), the NRF through Science Research Center (SRC) (Grant No. 2018R1A5A6075964), and the Max Planck-POSTECH Center for Complex Phase Materials (Grant No. 2016K1A4A4A01922028). The work at Seoul National University was supported by the research program of the IBS (No. IBS-R009-G2). The work at the Helmholtz-Zentrum Dresden-Rossendorf, a member of the Eruopean Magnetic Field Laboratory, was supported by the Hochfeld-Magnetlabor Dresden. The Advanced Light Source was supported by the Office of Basic Energy Science of the US Department of Energy under contract No. DE-AC02-05CH11231.

1. B. Keimer, S. A. Kivelson, M. R. Norman, S. Uchida, J. Zaanen, From quantum matter to high-temperature superconductivity in copper oxides. *Nature* **518**, 179–186 (2015).
2. R. M. Fernandes, P. P. Orth, J. Schmalian, Intertwined vestigial order in quantum materials: Nematicity and beyond. *Annu. Rev. Condens. Matter Phys.* **10**, 133–154 (2019).
3. S. V. Borisenko *et al.*, Pseudogap and charge density waves in two dimensions. *Phys. Rev. Lett.* **100**, 196402 (2008).
4. D. J. Rahn *et al.*, Gaps and kinks in the electronic structure of the superconductor 2*H*-$NbSe_2$ from angle-resolved photoemission at 1 K. *Phys. Rev. B Condens. Matter Mater. Phys.* **85**, 224532 (2012).
5. E. Rotenberg *et al.*, Electron states and the spin density wave phase diagram in Cr(110) films. *New J. Phys.* **7**, 114 (2005).
6. R. Yu, Q. Si, Orbital-selective Mott phase in multiorbital models for alkaline iron selenides $K_{1-x}Fe_{2-y}Se_2$. *Phys. Rev. Lett.* **110**, 146402 (2013).
7. L. de' Medici, G. Giovannetti, M. Capone, Selective Mott physics as a key to iron superconductors. *Phys. Rev. Lett.* **112**, 177001 (2014).
8. M. Yi *et al.*, Observation of temperature-induced crossover to an orbital-selective Mott phase in $A_xFe_{2-y}Se_2$ (A=K, Rb) superconductors. *Phys. Rev. Lett.* **110**, 067003 (2013).
9. M. Yi *et al.*, Observation of universal strong orbital-dependent correlation effects in iron chalcogenides. *Nat. Commun.* **6**, 7777 (2015).
10. J. A. Mydosh, P. M. Oppeneer, Colloquium: Hidden order, superconductivity, and magnetism: The unsolved case of URu_2Si_2. *Rev. Mod. Phys.* **83**, 1301–1322 (2011).
11. J. A. Mydosh, P. M. Oppeneer, P. S. Riseborough, Hidden order and beyond: An experimental-theoretical overview of the multifaceted behavior of URu_2Si_2. *J. Phys. Condens. Matter* **32**, 143002 (2020).
12. X. Zhu *et al.*, Transition of stoichiometric Sr_2VO_3FeAs to a superconducting state at 37.2 K. *Phys. Rev. B Condens. Matter Mater. Phys.* **79**, 220512 (2009).
13. I. I. Mazin, Sr_2VO_3FeAs as compared to other iron-based superconductors. *Phys. Rev. B Condens. Matter Mater. Phys.* **81**, 020507 (2010).
14. K.-W. Lee, W. E. Pickett, Sr_2VO_3FeAs: A nanolayered bimetallic iron pnictide superconductor. *Europhys. Lett.* **89**, 57008 (2010).
15. J. M. Ok *et al.*, Frustration-driven C_4 symmetric order in a naturally-heterostructured superconductor Sr_2VO_3FeAs. *Nat. Commun.* **8**, 2167 (2017).
16. G.-H. Cao *et al.*, Self-doping effect and successive magnetic transitions in superconducting $Sr_2VFeAsO_3$. *Phys. Rev. B Condens. Matter Mater. Phys.* **82**, 104518 (2010).
17. F. Hummel, Y. Su, A. Senyshyn, D. Johrendt, Weak magnetism and the Mott state of vanadium in superconducting Sr_2VO_3FeAs. *Phys. Rev. B Condens. Matter Mater. Phys.* **88**, 144517 (2013).
18. A. E. Böhmer *et al.*, Origin of the tetragonal-to-orthorhombic phase transition in FeSe: A combined thermodynamic and NMR study of nematicity. *Phys. Rev. Lett.* **114**, 027001 (2015).
19. M. Rotter *et al.*, Spin-density-wave anomaly at 140 K in the ternary iron arsenide $BaFe_2As_2$. *Phys. Rev. B Condens. Matter Mater. Phys.* **78**, 020503 (2008).
20. R. M. Fernandes, A. V. Chubukov, J. Schmalian, What drives nematic order in iron-based superconductors? *Nat. Phys.* **10**, 97–104 (2014).
21. X. Chen, P. Dai, D. Feng, T. Xiang, F.-C. Zhang, Iron-based high transition temperature superconductors. *Natl. Sci. Rev.* **1**, 371–395 (2014).
22. M. Yi, Y. Zhang, Z.-X. Shen, D. Lu, Role of the orbital degree of freedom in iron-based superconductors. *npj Quantum Mater.* **2**, 57 (2017).
23. T. Qian *et al.*, Quasinested Fe orbitals versus Mott-insulating V orbitals in superconducting $Sr_2VFeAsO_3$ as seen from angle-resolved photoemission. *Phys. Rev. B Condens. Matter Mater. Phys.* **83**, 140513 (2011).
24. Y. K. Kim *et al.*, Possible role of bonding angle and orbital mixing in iron pnictide superconductivity: Comparative electronic structure studies of LiFeAs and Sr_2VO_3-FeAs. *Phys. Rev. B Condens. Matter Mater. Phys.* **92**, 041116 (2015).
25. P. Richard, T. Sato, K. Nakayama, T. Takahashi, H. Ding, Fe-based superconductors: An angle-resolved photoemission spectroscopy perspective. *Rep. Prog. Phys.* **74**, 124512 (2011).
26. Y.-M. Xu *et al.*, Fermi surface dichotomy of the superconducting gap and pseudogap in underdoped pnictides. *Nat. Commun.* **2**, 392 (2011).
27. T. Shimojima *et al.*, Pseudogap formation above the superconducting dome in iron pnictides. *Phys. Rev. B Condens. Matter Mater. Phys.* **89**, 045101 (2014).
28. K. Tanaka *et al.*, Distinct Fermi-momentum-dependent energy gaps in deeply underdoped Bi2212. *Science* **314**, 1910–1913 (2006).
29. T. Kondo, R. Khasanov, T. Takeuchi, J. Schmalian, A. Kaminski, Competition between the pseudogap and superconductivity in the high-$T(c)$ copper oxides. *Nature* **457**, 296–300 (2009).
30. R. M. Fernandes, S. A. Kivelson, E. Berg, Vestigial chiral and charge orders from bidirectional spin-density waves: Application to the iron-based superconductors. *Phys. Rev. B* **93**, 014511 (2016).
31. M. H. Christensen, J. Kang, R. M. Fernandes, Intertwined spin-orbital coupled orders in the iron-based superconductors. *Phys. Rev. B* **100**, 014512 (2019).
32. Z. P. Yin, K. Haule, G. Kotliar, Kinetic frustration and the nature of the magnetic and paramagnetic states in iron pnictides and iron chalcogenides. *Nat. Mater.* **10**, 932–935 (2011).
33. T. Terashima *et al.*, Magnetotransport studies of $EuFe_2As_2$: The influence of the Eu^{2+} magnetic moments. *J. Phys. Soc. Jpn.* **79**, 103706 (2010).
34. S. Tatematsu, E. Satomi, Y. Kobayashi, M. Sato, Magnetic ordering in V-layers of the superconducting system of $Sr_2VFeAsO_3$. *J. Phys. Soc. Jpn.* **79**, 123712 (2010).
35. P. Ghaemi, T. Senthil, Higher angular momentum Kondo liquids. *Phys. Rev. B Condens. Matter Mater. Phys.* **75**, 144412 (2007).
36. H. Weber, M. Vojta, Heavy-fermion metals with hybridization nodes: Unconventional Fermi liquids and competing phases. *Phys. Rev. B Condens. Matter Mater. Phys.* **77**, 125118 (2008).
37. J. M. Ok *et al.*, Strong antiferromagnetic coupling in a heterostructured superconductor Sr_2VO_3FeAs. arXiv [Preprint] (2020). https://arxiv.org/abs/2010.01752 (Accessed 27 June 2021).
38. P. Dai, J. Hu, E. Dagotto, Magnetism and its microscopic origin in iron-based high-temperature superconductors. *Nat. Phys.* **8**, 709–718 (2012).
39. C. Ulrich *et al.*, Magnetic neutron scattering study of YVO_3: Evidence for an orbital Peierls state. *Phys. Rev. Lett.* **91**, 257202 (2003).
40. I. V. Solovyev, Lattice distortion and magnetism of 3*d*-t_{2g} perovskite oxides. *Phys. Rev. B Condens. Matter Mater. Phys.* **74**, 054412 (2006).
41. M. Yi *et al.*, Symmetry-breaking orbital anisotropy observed for detwinned $Ba(Fe_{1-x}Co_x)_2As_2$ above the spin density wave transition. *Proc. Natl. Acad. Sci. U.S.A.* **108**, 6878–6883 (2011).
42. E. Fradkin, J. E. Hirsch, Phase diagram of one-dimensional electron-phonon systems. I. The Su-Schrieffer-Heeger model. *Phys. Rev. B Condens. Matter* **27**, 1680–1697 (1983).
43. H. Oh, S. Lee, Y. B. Kim, E.-G. Moon, Multiscale quantum criticality driven by Kondo lattice coupling in pyrochlore systems. *Phys. Rev. Lett.* **122**, 167201 (2019).
44. L. Kouwenhoven, L. Glazman, Revival of the Kondo effect. *Phys. World* **14**, 33–38 (2001).
45. Y. Bang, Pairing mechanism of heavily electron doped FeSe systems: Dynamical tuning of the pairing cutoff energy. *New J. Phys.* **18**, 113054 (2016).
46. P. J. Hirschfeld, Using gap symmetry and structure to reveal the pairing mechanism in Fe-based superconductors. *C. R. Phys.* **17**, 197–231 (2016).
47. T. Senthil, S. Sachdev, M. Vojta, Fractionalized fermi liquids. *Phys. Rev. Lett.* **90**, 216403 (2003).
48. R. Nandkishore, M. A. Metlitski, T. Senthil, Orthogonal metals: The simplest non-Fermi liquids. *Phys. Rev. B Condens. Matter Mater. Phys.* **86**, 045128 (2012).
49. S. Sachdev, Topological order, emergent gauge fields, and Fermi surface reconstruction. *Rep. Prog. Phys.* **82**, 014001 (2019).
50. E.-G. Moon, Deconfined thermal phase transitions with Z_2 gauge structures. arXiv [Preprint] (2018). https://arxiv.org/abs/1812.05621 (Accessed 16 March 2021).